

Technical Paper

Micromachining of coarse-grained aluminum including crystallographic effects



Sudhanshu Nahata^{1,2}, Nithyanand Kota^{1,3}, O. Burak Ozdoganlar*

^a Department of Mechanical Engineering, Carnegie Mellon University, Pittsburgh, PA 15213, USA

^b Department of Material Science and Engineering, Carnegie Mellon University, Pittsburgh, PA 15213, USA

^c Department of Biomedical Engineering, Carnegie Mellon University, Pittsburgh, PA 15213, USA

ARTICLE INFO

Keywords:

Crystallographic anisotropy
Orthogonal machining
Micromachining
Diamond turning
Coarse-grained aluminum

ABSTRACT

This paper presents an experimental analysis of the effects of crystallographic anisotropy of the workpiece material when machining coarse-grained pure aluminum under varying cutting conditions. Orthogonal cutting experiments were conducted on an instrumented planning setup, and cutting forces and surface roughnesses were measured in a full-factorial experimental design. Cutting speed, uncut chip thickness (feed), and tool rake angle were varied at multiple levels. To determine the effect of subsurface deformation left by the previous tool passes, experiments were conducted both with and without cleanup cuts that reduce the surface deformation. The effect of crystallographic orientations and their interaction with cutting conditions on the specific cutting energy, the effective coefficient of friction, and the resulting surface roughness were analyzed through an analysis of variance approach. It was concluded that the crystallographic anisotropy has a strong effect in specific cutting energies, with up to 360% variation across different grains. Similarly, the roughness of the machined surface was seen to vary significantly (up to 831%) with the crystallographic orientations. On the other hand, the effective coefficient of friction was observed to be insensitive to the changes in crystallographic orientations. Lastly, a significant (up to 45%) difference in specific cutting energies was observed between the cases with and without cleanup cuts, indicating the strong presence and the influence of sub-surface deformation.

1. Introduction

In a range of machining processes, such as in various mechanical micromachining (micromilling and microdrilling) and diamond turning processes, the interaction between the cutting tool and the metallic workpiece occurs primarily within a single grain or a few grains of the workpiece material. The plastic (shearing) deformation experienced on each grain (crystal) depends upon the orientation of the crystal, and the direction of cutting with respect to that orientation. Thus, the crystallographic anisotropy of the workpiece material strongly affects the cutting process, and the existing machining knowledge that assumes effectively isotropic material behavior becomes inapplicable. Specifically, there is a need for fundamental understanding and experimental data on the variation of machining forces and specific energies, effective coefficient of friction, and surface roughnesses across

different grains under varying cutting conditions and tool geometry.

A suitable method for experimentally analyzing such effects is to perform orthogonal machining experiments on single-crystals and coarse grained polycrystals. A number of experimental studies have confirmed that machining response, including machining forces [1–13] and surface roughness [2,3,14,6,9], depends upon the crystallographic orientation. Experiments were conducted in both plunge-turning [5,12,6] and planning configurations [1–3,15,4,16,17,7,9,14,10,11,13] on single-crystal and coarse grained polycrystal metals, including aluminum [2,4–7,10,14,11,13], and copper [1,3,5,7,9]. The results from the planning studies showed that the anisotropy of face-centered cubic (fcc) crystals strongly affects the machining forces, inducing up to 312% variation in machining forces at different crystallographic orientations for a given zone axis [13]. The results from the turning studies about the [0 0 1] axis showed a repeatable four-fold symmetry expected from

* Corresponding author at: Department of Material Science and Engineering, Carnegie Mellon University, Pittsburgh, PA 15213, USA.

E-mail address: ozdoganlar@cmu.edu (O.B. Ozdoganlar).

¹ Both authors contributed equally to this manuscript.

² Currently at ASML US, CT.

³ Currently at Adobe Inc., CA.

the crystallographic symmetry of the [0 0 1] zone axis [5].

Although there exists a consensus in the literature that the crystallographic anisotropy of metals strongly affects their machining response [18,4–7,9–13], quantitative observations on the effects of crystallographic anisotropy have been limited to only a few sets of cutting conditions and crystallographic orientations. Furthermore, although the subsurface deformation created by previous tool passes could change the machining response [11,19,20] and its relationship with the crystallographic anisotropy significantly, no work in the literature provided comprehensive experimental data on the interaction effects between the subsurface damage and crystallography.

This paper presents an experimental investigation on the effects of crystallographic anisotropy during orthogonal machining of coarse-grained pure aluminum. Orthogonal machining (planning) is chosen to simplify the kinematics of the process when analyzing the crystallographic effects. Experiments are conducted under varying feed (uncut chip thickness) values, cutting speeds, and rake angles, and the variations of machining forces (analyzed in terms of specific cutting energy and effective coefficient of friction) and surface roughnesses across different grains are measured. To analyze the effect of the subsurface damage in the presence of crystallographic anisotropy, experiments were conducted both with and without cleanup cuts, which alleviate the subsurface deformation.

2. Experimental methods

2.1. Experimental facility

To conduct the experiments presented in this work, a sliding microtome was modified to create an orthogonal planning system shown in Fig. 1(a). The microtome consists of a vertical stage with 1 μm resolution, and a horizontal slide capable of moving at velocities ranging from 1 mm/s to 100 mm/s. A tool post was constructed on the vertical stage from extruded aluminum frames, and the tool is attached to the tool post through an adaptor plate. Therefore, the uncut chip thickness can be specified by moving the vertical stage. The workpiece was attached to the horizontal slide, which provides the cutting velocity. A force dynamometer (Kistler 9256C1) attached between the adaptor plate and the tool post facilitates measuring the three mutually-orthogonal machining force components (see Fig. 1(a)).

The stiffness of the structural loop is critical to ensure that the actual and specified uncut chip thickness (feed) values do not differ significantly due to deflections under machining forces. A set of preliminary tests was conducted to assess the difference between the specified and actual uncut chip thickness values: A protruded wall-like feature was machined on an aluminum 7075 workpiece (see Fig. 2) at different feed values, and the corresponding vertical forces were recorded. Between each cut, a negative replica of the wall was created (see Fig. 2) using a repliset system that, according to the manufacturer, is capable of replicating features less than 0.1 μm . The actual uncut chip thickness values were determined by measuring the change in feature depth on the replicas using white-light interferometry (WYKO).

Table 1 provides the actual and prescribed uncut chip thickness values, and the associated vertical forces. It is seen that the difference between the measured and prescribed uncut chip thickness values never exceeded 1 μm for any of the test conditions. It is noted that the vertical forces considered in this evaluation study well-covers the range of vertical (thrust) forces measured during the experimentation on coarse-grained aluminum. Therefore, we expect the actual uncut chip thickness values during the experiments to be within 1 μm of the prescribed values.

2.2. Tool characterization

The cutting edge sharpness, as measured by the radius of the cutting edge (the edge hone), has a profound effect in cutting mechanics. In

particular, larger edge radii produces increased ploughing and more extensive deformations near the tool edge [21]. To minimize the aforementioned complexities arising from the use of non-sharp tools, especially while machining at the micro-scale, a custom made single crystal diamond tool was used during the experiments. The diamond tool has an edge length (cutting width) of 2.5 mm and an included angle of 60°. The rake angles can be selected within 0°–25° range by using different tool-holder adaptors, while still maintaining a clearance angle of at least 5°. For a quantitative assessment of the tool, the edge radius was measured at eight locations along the edge with an atomic force microscope using the technique described in [13,22–25]. The measured edge radius was found to be 150.18 ± 20.26 nm along the cutting edge. Since the minimum uncut chip thickness during the experiments is 10 μm , this level of edge sharpness is considered to eliminate the effects of tool edge radius (and tool tip geometry) on cutting mechanics.

2.3. Workpiece characterization

Two samples of high purity aluminum (99.999%) were cut and polished to create workpieces with uniform widths (1.89 mm and 1.48 mm, respectively). To obtain coarse grained samples, the workpieces were subsequently annealed at 400 °C for 30 min. The resulting coarse grained workpieces (with grain lengths ranging from 1 mm to 10 mm along the length of the workpiece) were etched with hydrochloric acid to reveal the underlying grain structure. The grains were then traced under oblique lighting conditions. Only those grains that span the entire width of the workpieces were indexed, and they were labeled as A_1 to A_6 for Workpiece 1 and B_1 to B_{11} for Workpiece 2.

Fig. 3 shows the side view of the two workpieces, where the grain boundaries are identified. To verify the location of grain boundaries, and to determine the orientation of each grain, orientation imaging microscopy (OIM) was used after the completion of the cutting tests. A typical orientation map obtained from OIM is overlapped on the workpiece image in Fig. 3. The measured orientations of each grain are given in Table 2 in terms of the three Euler angles.⁴ Fig. 4 shows cutting directions and cutting plane normals in terms of crystal coordinates projected on standard stereographic triangles. Since the orientations are well distributed over the stereographic triangles, the conclusions drawn from the experiments would not be biased toward specific crystallographic orientations.

2.4. Cutting conditions

The effects of cutting velocity (v), uncut chip thickness (h), and rake angle (α) on machining forces and surface finish were studied in the presence of crystallographic anisotropy. To also analyze the effect of subsurface deformation, experiments were conducted both with and without cleanup cut. The experimental conditions were selected based on the capabilities of the experimental setup in terms of cutting velocity, uncut chip thickness, width of cut and rake angles, and a full factorial design of experiments was conducted. The cutting conditions used during the study are provided in Table 3.

2.5. Experimental procedure

The experiments were performed on the coarse grained aluminum workpieces to enable analyzing the effects of cutting conditions and tool geometry on machining in the presence of crystallographic anisotropy. The adhesion of pure aluminum to the rake face of the diamond tool observed during the preliminary tests was eliminated by using a cutting fluid (Ecoline), which was applied on the rake face of the tool

⁴The orientation of grain B_6 could not be determined due to its insufficient size after the tests were completed.

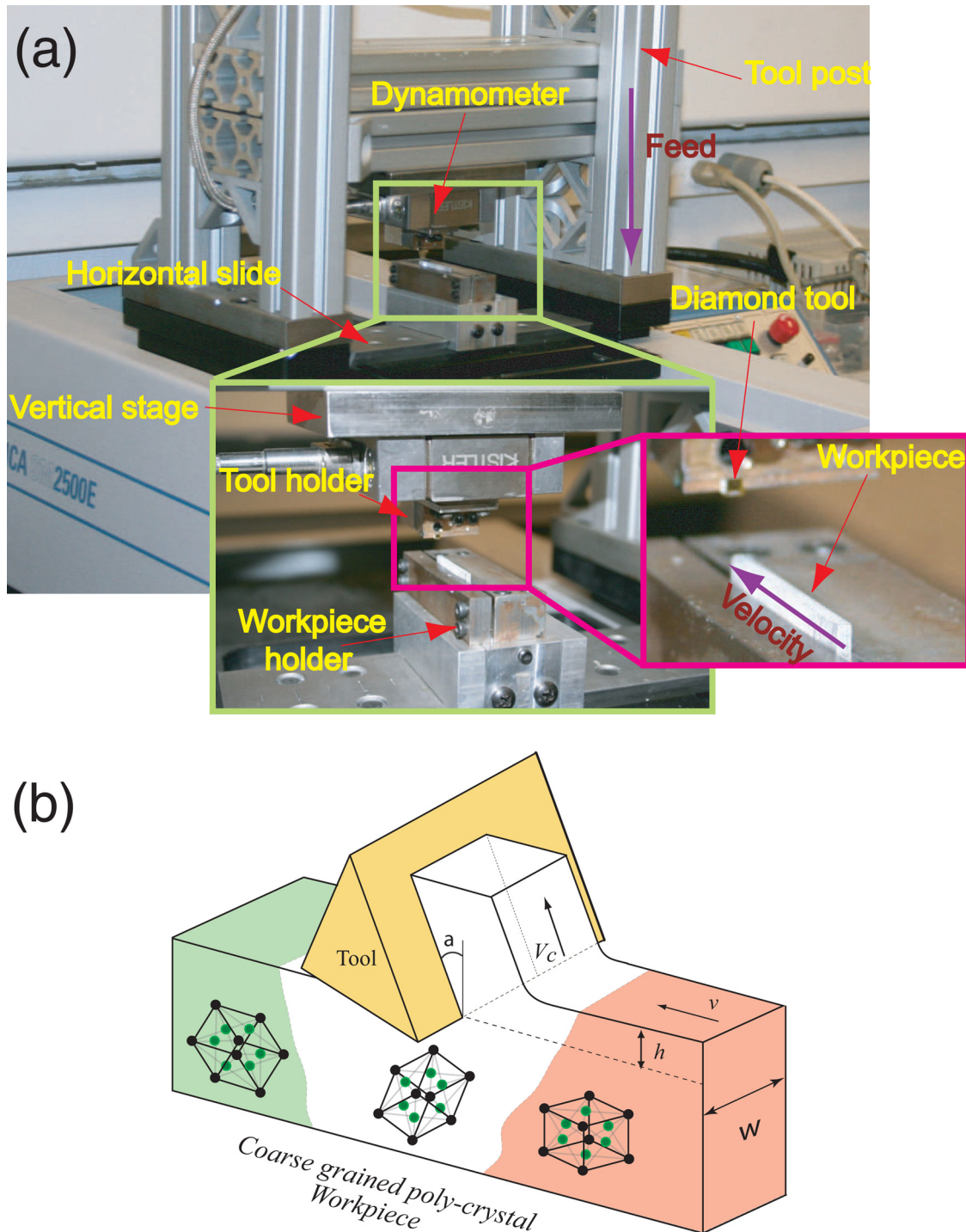


Fig. 1. (a) Planning apparatus and (b) schematic for machining coarse grained workpieces.

and the surface of the workpiece using a cotton swab prior to each test. The order of experiments were randomized, and two repetitions were performed for each set of conditions. The three-component force data was collected at a sampling rate of 5 kHz during the experiments. For each set of cutting conditions, experiments both with and without cleanup cuts were performed.

Prior study in the literature [19] has indicated that the depth of the subsurface deformation imparted by the cutting process does not exceed the uncut chip thickness of the previous tool pass. Hence, in this work, the subsurface damage was mitigated significantly by performing multiple $2\text{ }\mu\text{m}$ cleanup cuts before each with-cleanups test, with a total

removal depth equal to the uncut chip thickness of the previous cut.

The roughness of the cut surfaces were analyzed only for the with-cleanups tests. A replica-based roughness measurement procedure was followed to avoid removing the workpiece from the experimental setup between tests: A replica of the cut surface was made using the Repliset system after every cut (in a similar manner to that shown in Fig. 2). The roughness measurements were later taken from the replicas using an optical profilometer (Zygo NewView 7300). The measurements were performed over an area of $180\text{ }\mu\text{m} \times 50\text{ }\mu\text{m}$ on the center of each grain along the length direction from the mid section of the workpiece width.

As per the manufacturer, the Repliset system is accepted by ASTM

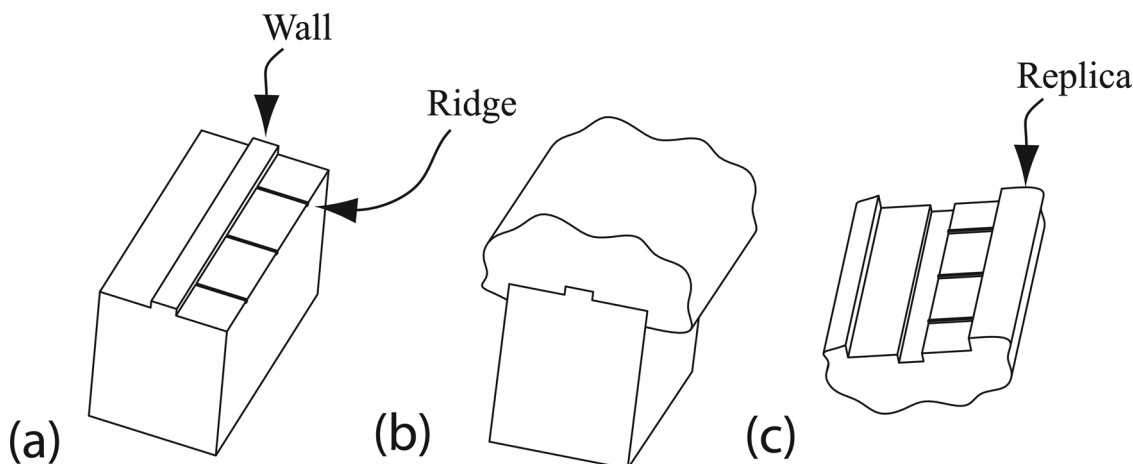


Fig. 2. Replica based measurement procedure (a) aluminum workpiece with the wall feature, (b) replica material applied on top of the workpiece, and (c) replica removed for measurement. The process is repeated after each cut and the depth of the replicas are measured at ridge locations to obtain the actual uncut chip thickness.

Table 1

Results of the preliminary study to measure the difference between the actual and prescribed uncut chip thicknesses.

Test	Prescribed (μm)	Measured (μm)	Vertical force (N)
1	10	10.1	4.8
2	10	10.8	4.6
3	20	19.9	5.4
4	20	20.5	5.6
5	40	40.9	9.9
6	40	39.9	11

to be used for surface characterization based on ASTM standard E 1351 “Standard Practice for Production and Evaluation of Field Metallographic Replicas”. To confirm the accuracy of the RepliSet system in providing average surface roughness (R_a) of a replicated surface, we conducted a set of experiments. For this purpose, we micromachined an aluminum coupon (see Fig. 2) and created a wall feature. A replica of the wall is made using the RepliSet and the roughness of the cut surface is measured from both the machined sample and its replica. The measurement is made over an area of $180 \mu\text{m} \times 50 \mu\text{m}$ using a white-light interferometer (Zygo NewView 7300). The interferometer outputs a 3D profile of the measurement area, from which the user can obtain the S_a or R_a . The measurements indicated that the average surface roughness (R_a) measured from the actual surface and its replica differs by less than 4 nm. Considering the measured R_a values of micromachined polycrystalline samples ranged from 32 nm to 265 nm, we considered the RepliSet system provides the required level of accuracy for our analyses.

3. Results and discussion

The kinematics of orthogonal machining and associated machining forces are depicted in Fig. 5, where F_c , F_t , and F are the cutting, the thrust and the resultant (machining) forces, respectively. ϕ and β represent the shear angle and the friction angle, respectively in Fig. 5. To represent the cutting process in a normalized fashion, the experimental machining forces are divided by the uncut chip area, which is equal to the product of the width of the workpiece (width of cut) and the uncut chip thickness, to obtain the specific cutting (u_c) and specific thrust (u_t) energies.

A typical variation of specific energies across the grains along the length of the workpiece is shown for each workpiece in Fig. 6. To understand the variation between two consecutive runs, the average of the two runs (specific cutting energy) is shown as the solid line and the

range is expressed as filled patch centered about the mean. It is seen that for most grains, the two repetitions are within 5% of each other such that the filled patch makes it hard to read the mean values. Therefore, for some figures later in the text, only the mean is shown for brevity. For presenting the specific energy data, the length axis is normalized to the total sample length, and shown as a percentage. The observed abrupt changes on specific energy signatures across the grain boundaries are due to the anisotropy of consecutive crystals, rather than a direct effect from the grain boundaries themselves, which are only a few atoms thick.

As the cutting process transitions from one grain to another, the stress field ahead of the tool could affect to forces. This may induce uncertainty to source of the forces, i.e., whether they arise entirely from the current grain or include effects from the cutting process on the previous grain. Considering the sharpness of the diamond tool, we expect the stress field ahead of the tool to be small, possibly equal to or less than the chip thickness [26,27]. Therefore, such transient effects are expected to diminish quickly. In this work, we chose a more conservative approach to eliminate the uncertainty arising from grain-to-grain transition effects: we calculated the average specific energy values for a given grain by using forces averaged over the half the (cutting direction) length of that grain centered at the mid-point of the grain length.

In general, the grain-to-grain variations of specific thrust energies were seen to follow those of specific cutting energies (see Fig. 6). However, while the specific cutting energy is always positive, the specific thrust energy exhibits both positive and negative values due to the force equilibrium in orthogonal cutting at higher rake-lower friction conditions. For this reason, a quantitative comparison between the maximum and minimum specific thrust energies across grain orientations is not informative. Therefore, the analysis presented here focuses mainly on the specific cutting energies and the effective coefficient of friction (μ), which is calculated as

$$\mu = \tan\left(\alpha + \arctan\left(\frac{u_t}{u_c}\right)\right). \quad (1)$$

Together, the specific cutting energy (cutting force) and the effective coefficient of friction completely describe the kinematics of the orthogonal cutting process, allowing other force components to be calculated with the knowledge of the rake angle. It is important to note that the observed variations of effective coefficient of friction are not accompanied with physical explanations of the effects. This is because the calculation of the effective coefficient of friction is only provided to characterize the change in cutting force ratios, rather than the changes

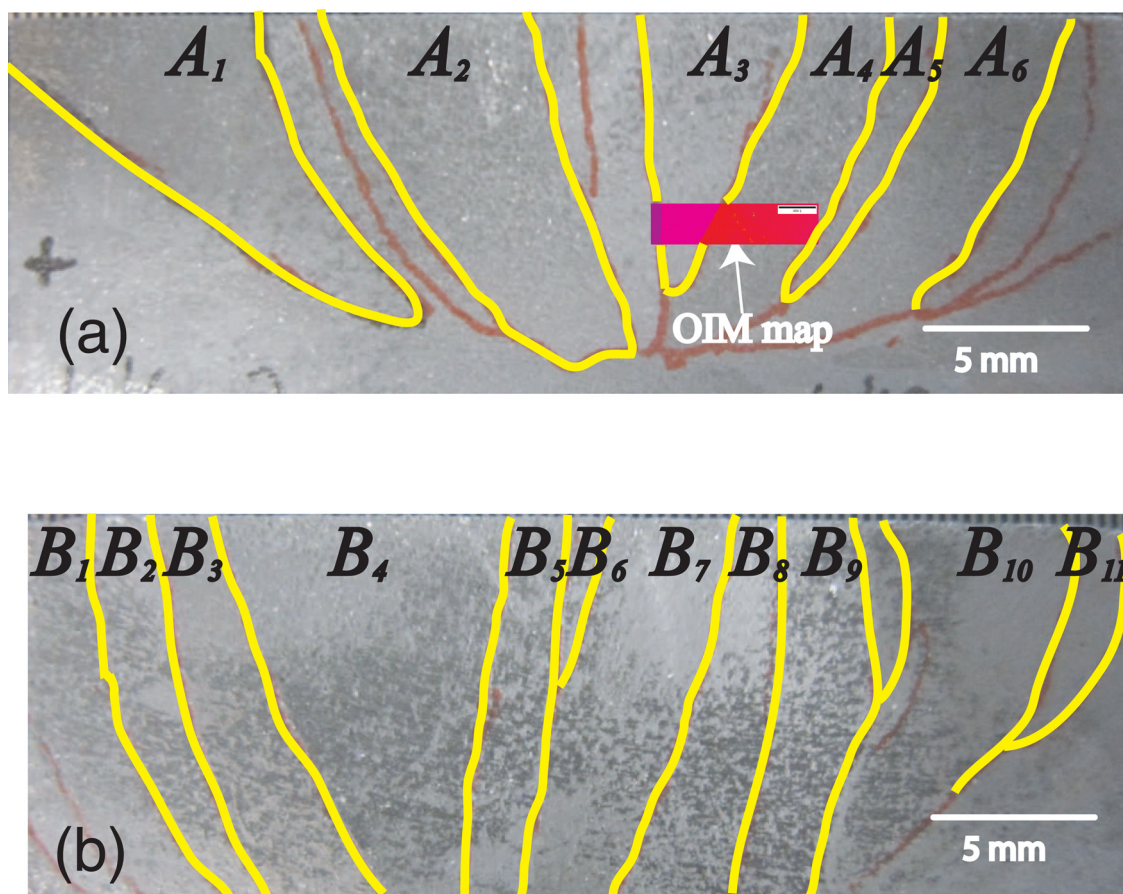


Fig. 3. (a) Workpiece 1 and (b) Workpiece 2 with traced grain maps.

Table 2
Orientations of the grains.

Grain number	φ_1 (°)	ϕ (°)	φ_2 (°)
A ₁	53	38	327
A ₂	131	14	265
A ₃	84	28	316
A ₄	36	12	294
A ₅	45	11	316
A ₆	28	18	312
B ₁	343	13	35
B ₂	341	10	16
B ₃	333	9	53
B ₄	283	26	36
B ₅	278	29	85
B ₆			
B ₇	246	17	171
B ₈	305	42	36
B ₉	296	51	46
B ₁₀	215	49	147
B ₁₁	220	40	163

in actual friction characteristics. Although one may suggest physical changes in actual coefficient of friction and the friction force due to grain-to-grain variations, such analyses are beyond the scope of the current work.

To assess the repeatability of the experimental results and their statistical significance, a multi-variate analysis of variance (ANOVA) was performed on the average specific cutting energies and the effective coefficients of friction. In this analysis, the statistical significance of a factor was decided considering a 95% confidence interval (a *p*-value less than 0.05) [28]. A preliminary analysis including all the interaction effects indicated that, although some high-level interaction effects were

statistically significant, their *F* values (normalized magnitudes) were considerably smaller than those of the main and two-way interaction effects. Therefore, only the main and two-way interaction effects were considered in this study.

The factors used in the ANOVA analysis included crystallographic orientation (17 levels), rake angle (3 levels), cutting velocity (2 levels), uncut chip thickness (3 levels), and cleanup status (2 levels – with and without). Table 4 presents the results from the ANOVA analysis for the specific cutting energy and the effective coefficient of friction, where the statistically *insignificant* values are italicized: It is seen that except the interaction between orientation and cutting velocity, and that between velocity and uncut chip thickness, all the main and interaction effects are statistically significant for the specific cutting energy. For the effective coefficient of friction, three interaction effects were not statistically significant.

3.1. Machining surfaces after cleanup cuts

In this section, the effects of cutting conditions and their interaction with the crystallographic anisotropy are analyzed in detail for surfaces that are prepared by performing the cleanup cuts.

3.1.1. The main effects of crystallographic anisotropy

The main-effect plot for the crystallographic orientation on specific cutting energy is given in Fig. 7(a). This plot averages the specific cutting energies over all the conditions: Although the exact variation between the orientations depends upon the specific set of cutting conditions, the main effect plot provides an overall perspective on the effect of anisotropy. The averaged specific cutting energies were seen to vary significantly with the crystallographic orientation. The specific cutting energy was seen to vary by as much as 360% (between grains B₁

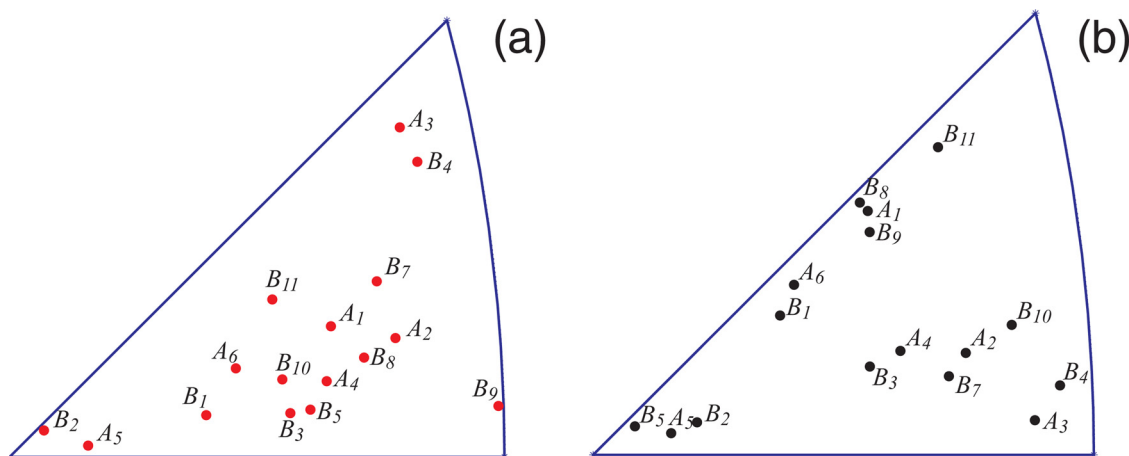


Fig. 4. Projections of (a) cutting plane normals and (b) cutting directions, in the standard stereographic triangle.

Table 3
Experimental conditions for orthogonal machining studies.

Uncut chip thickness (μm), h	10, 20, 40
Rake angle ($^\circ$), α	0, 10, 25
Cutting speed (mm/s), v	10, 50

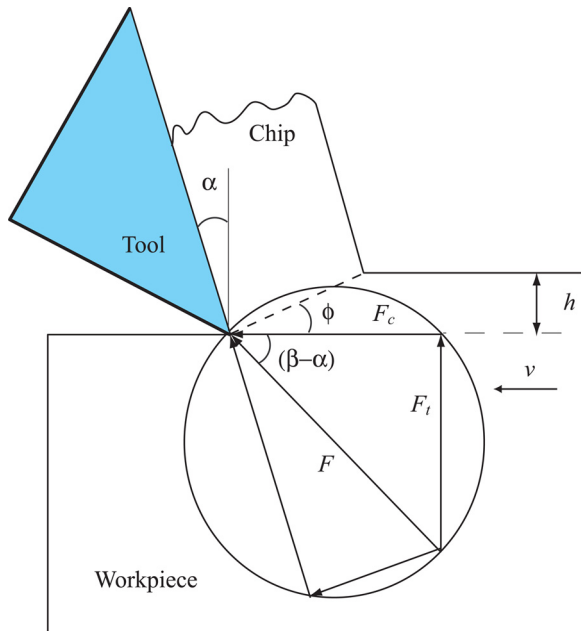


Fig. 5. Kinematics of the orthogonal cutting and the Merchant's force circle diagram.

and B_2).

The strong effect of crystallographic anisotropy arises from the dependence of the deformation behavior of crystals upon the arrangement of slip systems with respect to the cutting orientation (both the plane normal and the cutting direction). Some researchers [29,30] attempted to capture the effect of crystallographic anisotropy by calculating the Schmid factors along the direction of the resultant machining force. To determine the variation of the Schmid factor during the experiments presented here, the resultant force magnitude and direction was calculated from the measured cutting and thrust forces. Subsequently, the associated Schmid factors for the average resultant force directions for each orientation were determined and presented in Fig. 8. It is seen that the maximum variation in Schmid factors was 16%. Thus, the observed

variations due to crystallographic anisotropy cannot be explained through the Schmid factors. This is an expected result, since the Schmid-factor based models assume that the deformation occurs only along a single slip system: In reality, fcc metals have 12 slip systems, and generally five independent slip systems must be activated simultaneously to accommodate an arbitrary deformation. Prediction and quantitative analysis of the effect of anisotropy under such conditions would require more elaborate plasticity-based models of the machining process [31,32], including multiple slip, hardening, and crystal rotation effects.

The variation in effective coefficient of friction with orientation is shown in Fig. 7 using the main effect plot obtained by averaging over uncut chip thicknesses, cutting velocities, and rake angles. Except for three crystals, the average coefficient of friction was observed to be within a narrow range of 0.07–0.1 (corresponding to 4° – 5.7° in terms of friction angle). On closer observation and comparing with the main effects plot for the specific cutting energy, the three outliers were seen to be for orientations whose specific cutting energies are the lowest (A_2 , B_1 , B_3). It is possible that unbiased noise affects those low specific energy values, and thus, prevents accurate calculation of the effective coefficient of friction. Overall, within the range of parameters tested in this study, the variation of effective coefficient of friction with crystallographic orientation was seen to be minimal. This indicates that the cutting and thrust forces are well-correlated across different crystallographic orientations.

3.1.2. The effects of rake angle

The main effect of the rake angle on specific cutting energy is seen in Fig. 7(b). It is seen that the increasing the rake angle reduces the specific cutting energy. The average specific cutting energy at 0° rake angle is observed to be higher than that at 25° rake angle by approximately 250%. This effect is similar to that seen in machining of effectively isotropic materials, and is due to the lower shear strains that reduce the extent of deformation at increased rake angles.

More detailed observations about the effects of rake angle can be made by analyzing the specific cutting energy signatures. Fig. 9 shows a sample data for both workpieces for 10 mm/s cutting speed at different uncut chip thickness values. The small shift observed in the individual grain signatures arises from the fact that the grain boundaries are not aligned with the feed direction, and thus, the starting and ending position of each crystal changes in subsequent tests. As concluded from the ANOVA analysis, the specific cutting energies were seen to reduce with increasing rake angles.

The interaction between the rake angle and orientation effects is critical to the current study. Fig. 10(a) presents the specific cutting energies for each rake angle by averaging the data over all the cutting speeds and uncut chip thicknesses. It is clear that the effect of rake

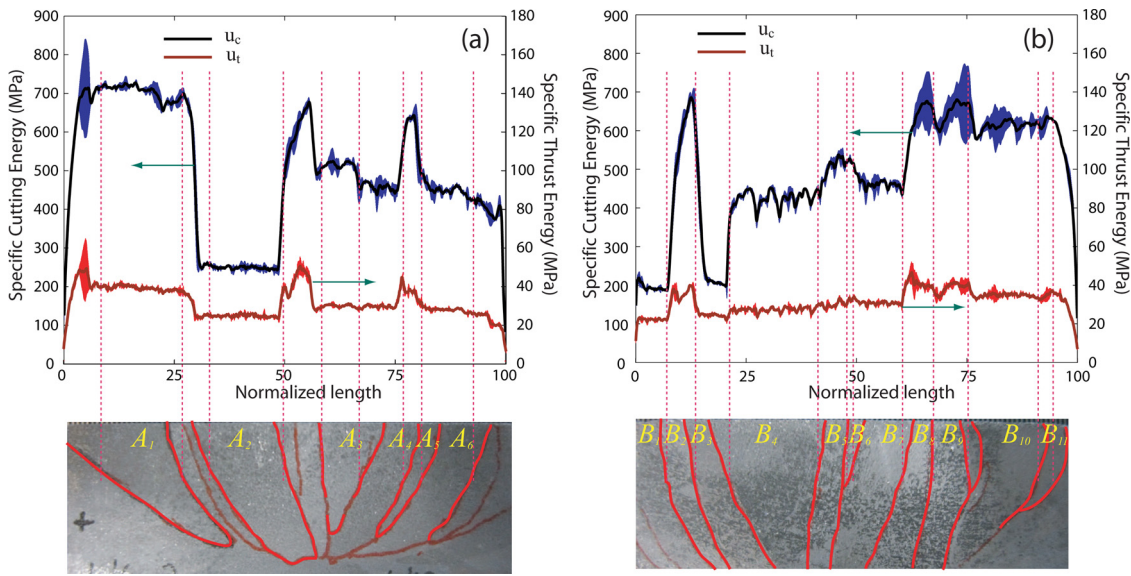


Fig. 6. Typical specific energy variations for (a) Workpiece 1 and (b) Workpiece 2, for 0° rake angle, 10 mm/s cutting velocity, and 40 μm uncut chip thickness. The green arrow indicates the corresponding y-axis applicable for the plot. The solid line represent the average of the two runs and the filled patch show the range centered about the mean.

Table 4

ANOVA results for the specific cutting energy and the effective coefficient of friction, where “**” denotes the interaction between two parameters.

Parameter	$P(u_c)$	$F(u_c)$	$P(\mu)$	$F(\mu)$
Orientation (e_1)	0.000	236.02	0.000	185.67
α (e_2)	0.000	3109.18	0.000	348.49
v (e_3)	0.000	63.26	0.000	16.61
h (e_4)	0.000	164.26	0.000	497.28
Cleanup (e_5)	0.000	1204.92	0.000	52.14
$e_1^*e_2$	0.000	50.89	0.000	23.60
$e_1^*e_3$	0.621	0.86	0.015	4.07
$e_1^*e_4$	0.000	8.17	0.000	42.89
$e_1^*e_5$	0.000	42.74	0.000	3.38
$e_2^*e_3$	0.003	5.77	0.009	4.69
$e_2^*e_4$	0.000	7.48	0.000	51.84
$e_2^*e_5$	0.000	275.64	0.213	1.55
$e_3^*e_4$	0.121	2.11	0.084	2.49
$e_3^*e_5$	0.000	16.38	0.072	3.25
$e_4^*e_5$	0.000	11.52	0.000	11.49

angle is not uniform across different crystallographic orientations: The maximum variation of average specific cutting energy was seen to be 415% at 0° rake angle and 250% at 25° rake angle. This implies that the variation of specific cutting energy arising from the anisotropy increases when the rake angle is reduced. In other words, the cutting process is more sensitive to effects of anisotropy at lower rake angles.

A possible explanation for the observed phenomena may be offered by considering the change in shear angle and shear strain with varying rake angle. Since a change in rake angle causes the average shear direction to change, even for the same cutting direction and crystal orientation, the plastic deformation during machining may vary significantly. Furthermore, the magnitude of strain experienced by the material also varies with the change in shear angle. Increased strains at lower rake angles, combined with the changes in orientation of the shear deformation, could result in increased variation in specific cutting energy with reducing rake angle.

The effective coefficient of friction (main effect) was seen to increase with increasing rake angles. The average value of the effective coefficient of friction was 0.16 at 25° rake angle and 0.08 at 0° rake angle. However, the variation of effective coefficient of friction across crystallographic orientations was found to be similar at all rake angles

(see Fig. 11(a)).

3.1.3. The effects of cutting velocity

As seen in Table 4 and Fig. 7(c), the main effect of the cutting velocity on specific cutting energy was seen to be statistically significant. Increased cutting speeds were observed to produce higher specific cutting energies. However, within the range of cutting velocities considered in this work, the effect of cutting velocity was seen to be small. Averaging over the crystallographic orientations, rake angles and uncut chip thicknesses, the specific cutting energy is only 8.6% higher at 50 mm/s than at 10 mm/s.

Changes in cutting velocities affects the cutting process through two opposing mechanisms. First, at increased strain rates experienced at higher cutting velocities, most metals show increased resistance against yielding, and thus, the specific cutting energies increase at higher velocities. Second, for a wide range of cutting speeds, increasing cutting velocity increases the workpiece temperatures, thereby softening the material, and thus, reducing the specific energies. For the relatively low-speed regime considered in the current tests, the former effect is considerably more dominant. More specifically, the effect of cutting speed is seen mainly on the stress distribution for a given applied strain. The resulting stress distribution is related to the strain rate through a power law relationship, typically in the form of $\sigma \propto (\dot{\gamma})^n$, where σ is the stress, $\dot{\gamma}$ is the strain rate, and n is the coefficient of rate sensitivity. The strain rate is directly proportional to the cutting velocity, and typical values of n for metals range from 10 to 30. Consequently, the effect of strain rate, and thus, the cutting velocity, on the stress response is relatively small. For instance, for coefficient of rate sensitivities within a range of 10–30, a five-fold increase in the cutting speed (strain rate) would result in a change of stress values within 5% and 17%. In the current set of experiments, the increase in specific cutting energy was seen to be 8.6% for a five-fold increase in the cutting velocity.

However, the interaction effect between the cutting velocity and crystallographic orientation on specific cutting energy was seen to be statistically insignificant. This can be explained by considering the stress-strain rate dependence described above: Since coefficient of rate sensitivity (n) is commonly independent of the orientation, the effect of speed is expected to be uniform across all orientations.

Although statistically significant, the cutting velocity was seen to have a little effect on the calculated average coefficient of friction (see Fig. 7(g)). In terms of friction angle the variation is less than 1° . The

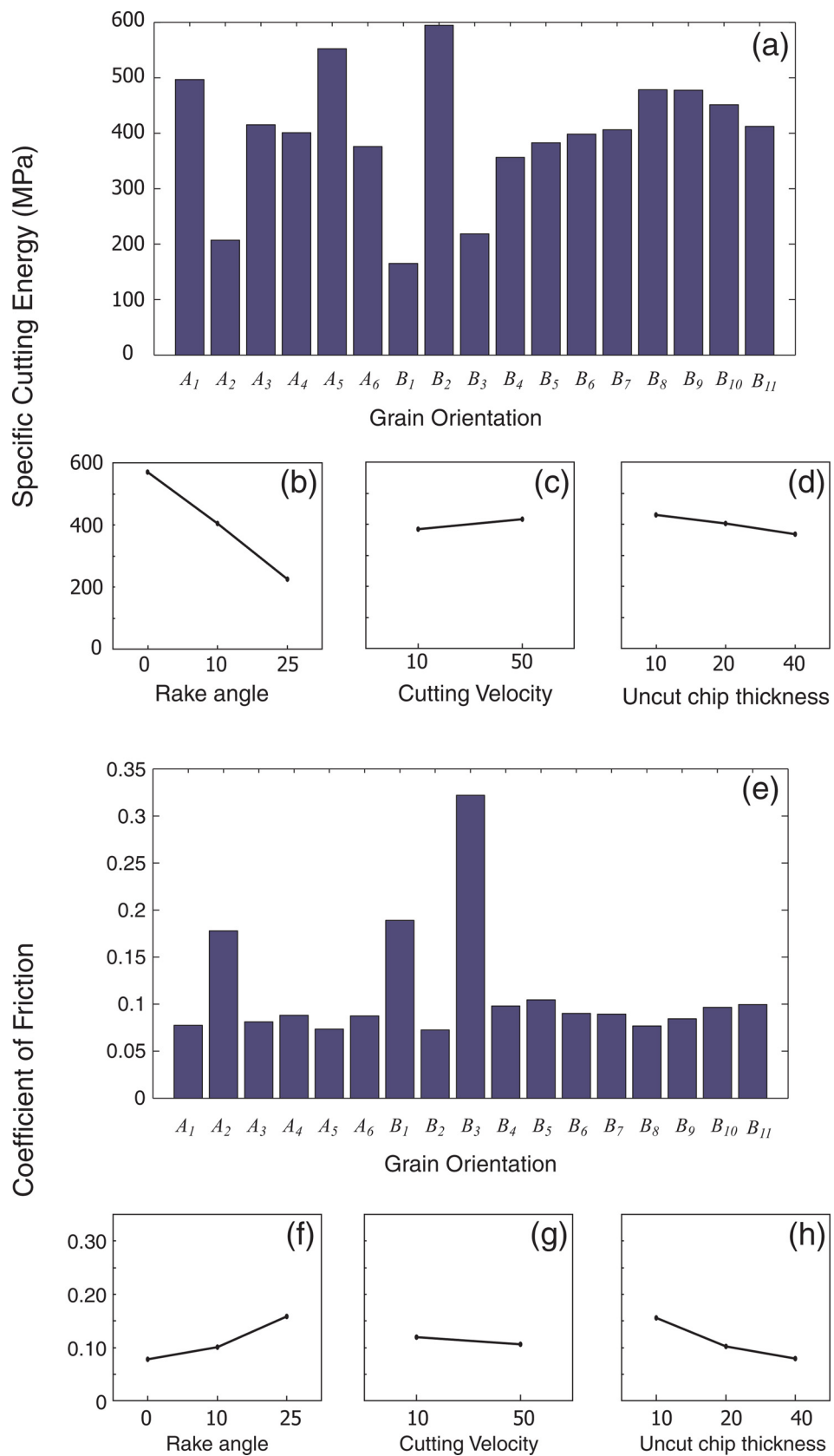


Fig. 7. Main effect plots for (a-d) Specific cutting energy and (e-h) effective coefficient of friction.

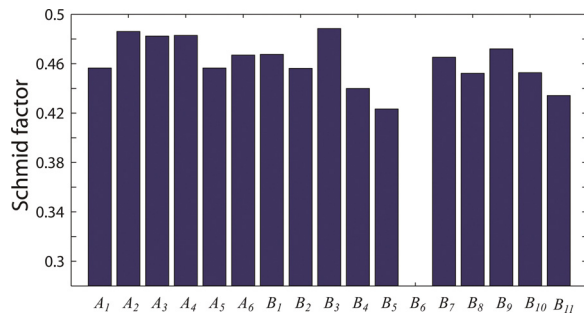


Fig. 8. Schmid factors for the resultant machining force directions. The orientation of grain B_6 could not be determined due to its insufficient size after the tests were completed.

variation of effective coefficient of friction across crystallographic orientations was found to be similar at all cutting velocities (see Fig. 11(b)).

3.1.4. The effects of uncut chip thickness

Table 4 and Fig. 7(d) shows that the main effect of the uncut chip thickness is statistically significant, and reduced uncut chip thickness results in increased specific cutting energies. The specific cutting energy at 10 μm was seen to be 17% higher than that at 40 μm .

This phenomena, commonly referred to as the size effect, has been observed frequently in the machining literature for effectively isotropic materials, e.g., in [33–36]. Researchers have attributed the size effect to the deformation characteristics of the material [34], the edge radius of the tool, and the fracture energy [37] necessary for chip separation. Due to the sharp diamond tool used in the current set of experiments, the effect of edge radius can be considered negligible. Both the fracture energy for chip separation and shearing behavior of the material could be orientation dependent, and may be responsible for the observed size effect. However, since the raise in specific cutting energy due to the

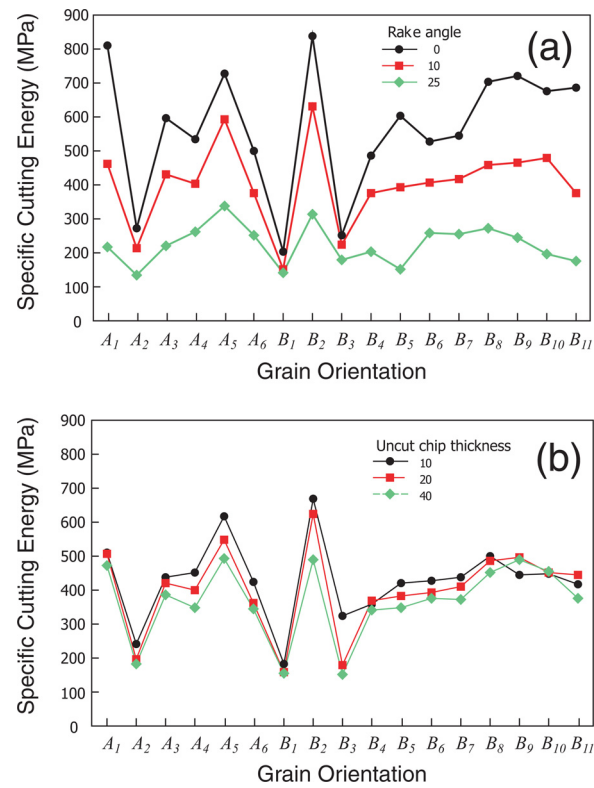


Fig. 10. Two-way interaction effects for specific cutting energy between (a) the grain orientation and the rake angle and (b) the grain orientation and the uncut chip thickness.

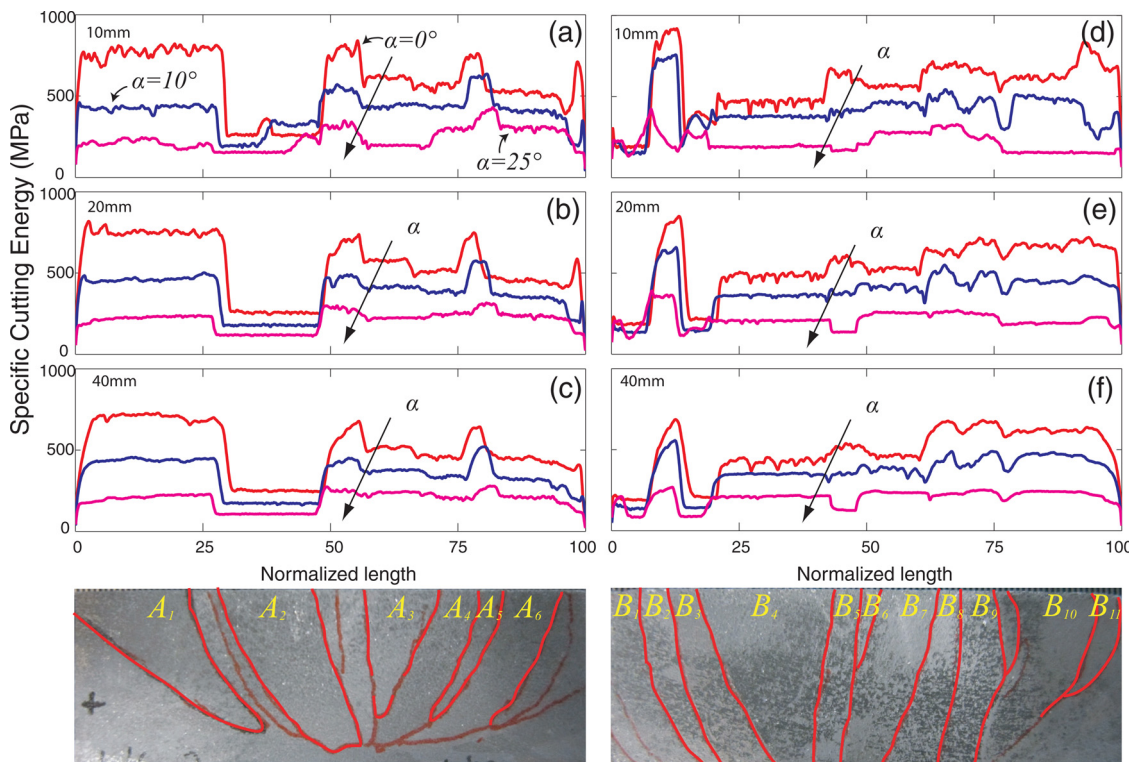


Fig. 9. Effect of rake angle on specific cutting energy signatures at various cutting conditions for (a–c) Workpiece 1 and (d–f) Workpiece 2, at 10 mm/s cutting velocity. The guidelines show the approximate midpoint of each grain for visual correlation only.

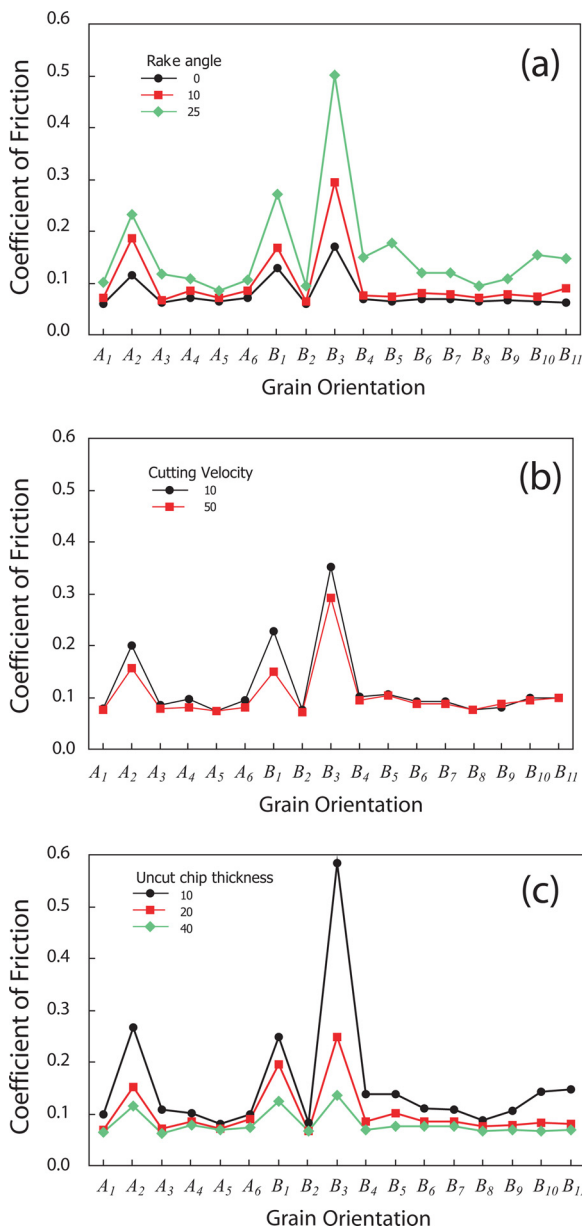


Fig. 11. Two-way interaction effects for specific cutting energy between (a) the grain orientation and the rake angle, (b) the grain orientation and the cutting velocity, and (c) the grain orientation and the uncut chip thickness.

uncut chip thickness reducing from 40 μm to 10 μm is approximately the same for each rake angle (18%, 16% and 19%, respectively at 0°, 10°, and 25° rake angles, respectively), it may be deduced that the amount of deformation does not affect the size effect significantly. Therefore, the observed size effect is most probably arising from the chip separation and new surface creation energies, which are commonly considered to be constant (and independent from the uncut chip thickness).

Fig. 12 shows the change in specific energies at three levels of uncut chip thickness for the two workpieces. It is seen here that the size effect is not uniform across different crystals. Therefore, there is an interaction effect between the uncut chip thickness and crystallographic orientation. The interaction effect could be visualized more effectively by averaging the specific energies for each uncut chip thickness over the cutting speed and rake angles, as shown in Fig. 10(b).

The effective coefficient of friction (main effect) was seen to reduce at higher uncut chip thicknesses. Fig. 7 shows that the average effective coefficient of friction at 10 μm uncut chip thickness is more than twice

(212%) of that at 40 μm uncut chip thickness. Furthermore, the variation of effective coefficient of friction with crystallographic orientations was similar (see Fig. 11(c)) at all uncut chip thicknesses.

3.1.5. Analysis of surface roughness

It was observed in the literature that machining different crystallographic orientations under the same cutting conditions could result in different surface roughnesses [14,6,9]. However, these experiments were performed on a very few orientations (and cutting conditions) [6], and only qualitative observations were made [14].

When machining an effectively isotropic material, the roughness of the generated surface depends upon the quality of the tool, kinematics of the process, and the vibrational response of the machining system. In the current study, the same tool is used for each test across different crystals, and since the wear of the diamond tool is negligible, the effect of tool quality on the surface roughness is uniform across the crystals and under different conditions. The kinematics of the process for given set of cutting conditions were also identical across different grains. Furthermore, at the steady state (away from the transition region from one crystal to another), the vibrational response of the structure could be assumed to be uniform.

When considering machining of single crystals and coarse-grained samples, the surface generation mechanism may play an important role. The generated surface is directly correlated with the orientation of the crystals, since the surface is generated by large plastic deformation of the material ahead of the tool edge combined with the separation of the chip from the workpiece through a fracture mechanism [38] (both of which are orientation dependent).

In the current study, the surface roughness was measured for all the cases with the cleanup cuts. The surface roughness data was analyzed thorough ANOVA based on the average surface roughness (R_a) values, as shown in Table 5, where the statistically *insignificant* effects are italicized. It is seen that the main effects of orientation, rake angle, cutting velocity, and uncut chip thickness, as well as various interaction effects are statistically significant.

The relevant main and interaction effects on average surface roughness are plotted in Fig. 13. As seen in Fig. 13(a), when averaged over all the cutting conditions, the surface roughness varies strongly with the crystallographic orientation. The largest variation was seen between grains B₂ and B₃, where the surface roughness of grain B₂ ($R_a = 265$ nm) was seen to be 831% higher than that of grain B₃ ($R_a = 32$ nm). When Figs. 13 and 7(a) are analyzed, a correlation between the roughness values and the specific energies may be observed: generally, higher roughness values are seen at orientations that result in higher specific energies.

Averaging over all the crystallographic orientations, the surface roughness was seen to increase with reducing rake angle, increasing uncut chip thickness, and reducing cutting speed. The average R_a values at 0° rake angle are higher than those at 25° rake angle by 90%, and the average R_a values at 40 μm uncut chip thickness are higher than those at 10 μm by 85%.

The interaction effect between the crystallographic orientation and the rake angle is shown in Fig. 13(e). It is seen that the effect of rake angle on average surface roughness varies at different crystallographic orientations. Similarly, the interaction effect between the crystallographic orientation and the uncut chip thickness is shown in Fig. 13(f). Generally, the surface roughness variations across the grains are seen to be smaller at lower uncut chip thicknesses. However, in many orientations, especially those that produce lower R_a values, the surface roughness variations does not change significantly with the uncut chip thickness. It is possible that this low level of surface roughness is an inherent limitation of the experimental setup, and is uniform across different grain orientations and uncut chip thicknesses.

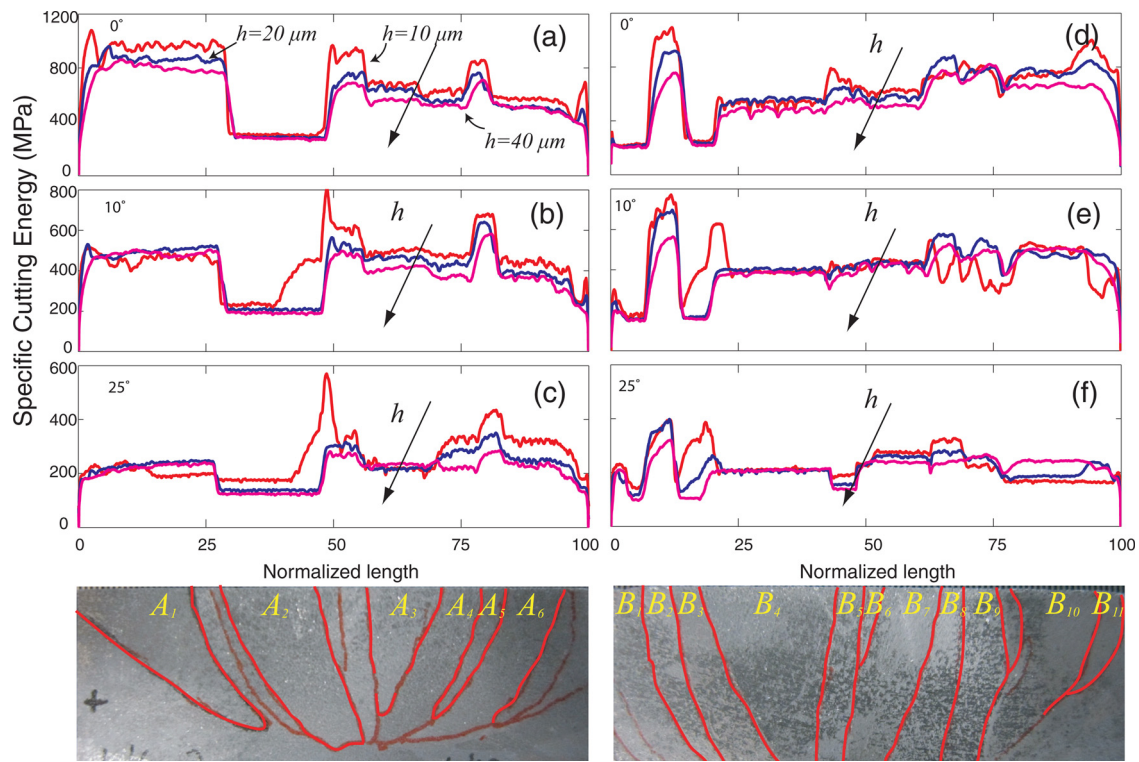


Fig. 12. Effect of uncut chip thickness on specific cutting energy signatures at various cutting conditions for (a–c) Workpiece 1 and (d–f) Workpiece 2, at 50 mm/s cutting velocity. The guidelines show the approximate midpoint of each grain for visual correlation only. Note the difference in the Y-axis scales.

Table 5
ANOVA results for the surface roughness, where “**” denotes the interaction between two parameters.

Parameter	$P(R_a)$	$F(R_a)$
Orientation (e_1)	0.000	47.07
α (e_2)	0.000	51.39
v (e_3)	0.023	5.20
h (e_4)	0.000	42.40
$e_1^*e_2$	0.000	3.38
$e_1^*e_3$	0.801	0.69
$e_1^*e_4$	0.001	2.16
$e_2^*e_3$	0.121	2.13
$e_2^*e_4$	0.013	3.23
$e_3^*e_4$	0.757	0.28

3.2. Machining surfaces without cleanup cuts

The presence of subsurface deformation from the previous cuts affects the material properties experienced during the subsequent cut [19]. As a result, both the deformation behavior and the specific energies vary due to existing subsurface deformation. For the results presented in the previous section, cleanup cuts were performed to minimize the effect of subsurface deformation. In this section, a systematic study is presented to assess the effect of subsurface deformation on specific energies in the presence of crystallographic anisotropy. As seen in Table 4, the main effect of the cleanup cuts, as well as its interaction effect with crystallographic orientations, are both statistically significant. Note that characterization of the sub-surface damage, both its nature and its extent, is beyond the scope of the current work. During experimentation, to obtain surfaces with reduced subsurface damage, we used multiple cuts with very small ($2 \mu\text{m}$) chip thicknesses, until a thickness equal to or more than the previous largest cut is removed. Based on the literature and our earlier work with 0° rake angle [19], the depth of damage due to mechanical removal (especially when using a sharp tool and at low cutting speeds) is about or less than one

times the uncut chip thickness. Thus, our approach limits the subsurface damage (for the “reduced subsurface damage” cases) to no more than $2 \mu\text{m}$.

A typical specific energy variation for a test with the cleanup cuts and the immediately following test (without cleanup cuts) are given in Fig. 14, where a 10° rake angle, a 10 mm/s cutting velocity, and a $40 \mu\text{m}$ uncut chip thickness were used. The main effect of the cleanup is shown in Fig. 15(a). Averaging across all test conditions, the cases with cleanup cuts resulted in a 31% higher specific cutting energy than those without cleanup cuts. Furthermore, the interaction effect between the cleanup and the rake angle is also statistically significant: This is possibly due to the larger deformations at lower rake angles causing the effect of cleanup cut to become larger at lower rake angles. The average increase in specific cutting energy with cleanup cuts is 8.7%, 29% and 45% at 25° , 10° , and 0° rake angles, respectively.

Although the interaction effect of uncut chip thickness and cleanup were seen to be statistically significant, the effect of cleanup is observed to be similar at different uncut chip thickness values. The cases without cleanup at $10 \mu\text{m}$ and $40 \mu\text{m}$ uncut chip thicknesses showed 29% and 26% reduction in average cutting specific energies, respectively, when compared to cases with cleanup cuts.

When compared to the experiments conducted with (after) cleanup cuts, the cases without cleanup cuts showed lower variation in specific cutting energy with crystallographic orientation, as shown by the two-way interaction effect depicted in Fig. 15(b). The standard deviation (with orientation) of average specific energy without cleanup cuts was equal to 68 MPa, whereas that with cleanup cut was equal to 115 MPa. This reduction in standard deviation indicates that larger subsurface deformation reduces the effect of anisotropy. Within the deformed regions of the subsurface, the lattice is not uniformly oriented [19]. The orientation of the crystal changes gradually from the surface. Therefore, during a cut without cleanup, the orientation of a large portion of the material begin removed is different from the original orientation of the bulk crystal.

For the effective coefficient of friction, the main effect of cleanup

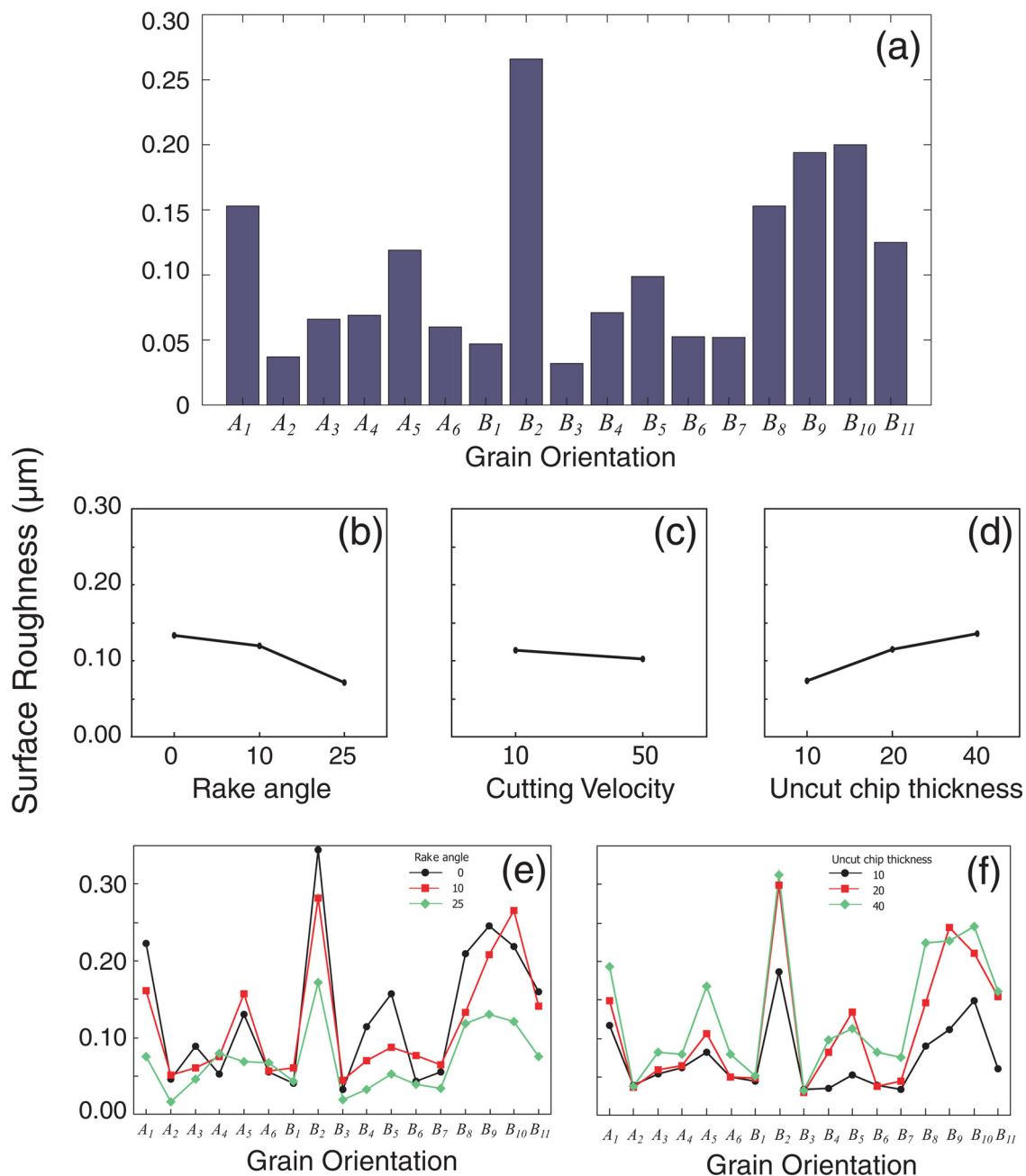


Fig. 13. (a-d) Main effect plots for surface roughness, and (e, f) two-way interaction effects for surface roughness between (e) the grain orientation and the rake angle, and (f) the grain orientation and the uncut chip thickness.

and its interaction effect with the uncut chip thickness are seen to be statistically significant. The effective coefficient of friction is seen to increase by 15% without cleanup, and the increase is seen to be higher at lower uncut chip thicknesses. The effective coefficient of friction without cleanup is seen to increase by 20%, 16%, and 5% at 10 μm , 20 μm , and 40 μm uncut chip thicknesses, respectively.

4. Summary and conclusions

This paper presented an experimental analysis of orthogonal machining of coarse-grained aluminum including the crystallographic anisotropy. A planning setup is used to conduct experiments with a full-factorial design including 17 crystallographic orientations and varying cutting conditions, and the specific cutting energies and effective coefficients of friction were calculated from the measured forces. Multi-

variate analysis of variance was used to assess the repeatability and statistical significance of different parameters and their interaction with crystallographic orientations. The tests with and without cleanup cuts were performed to determine the effect of subsurface damage and its interaction with crystallographic effects.

The effect of crystallographic anisotropy on specific cutting energy was seen to be strong, resulting in 360% variation for the experimental conditions and crystallographic orientations considered in this work. The effects of cutting conditions, when averaged over crystallographic orientations, was seen to follow those seen during machining of isotropic materials: the specific cutting energy was seen to increase with reducing rake angle, increasing cutting velocity, and reducing uncut chip thickness.

The effect of anisotropy was seen to be stronger at lower rake angles; the maximum variation in specific cutting energy was 415% at 0°

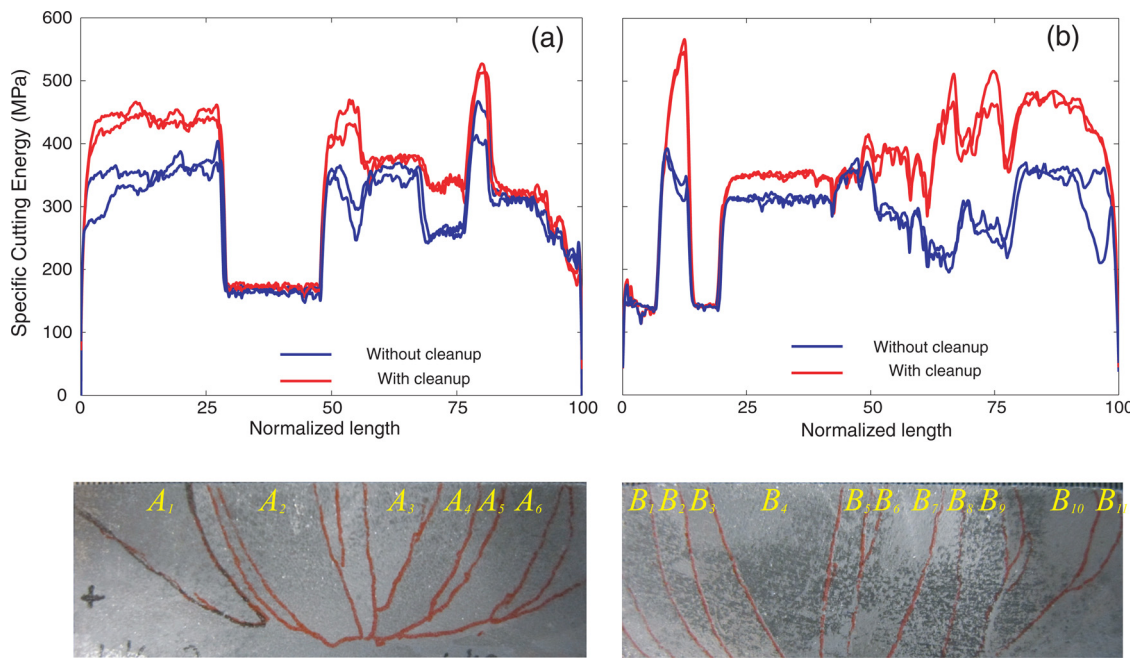


Fig. 14. Typical effect of cleanup cut on specific cutting energy for (a) Workpiece 1 and (b) Workpiece 2.

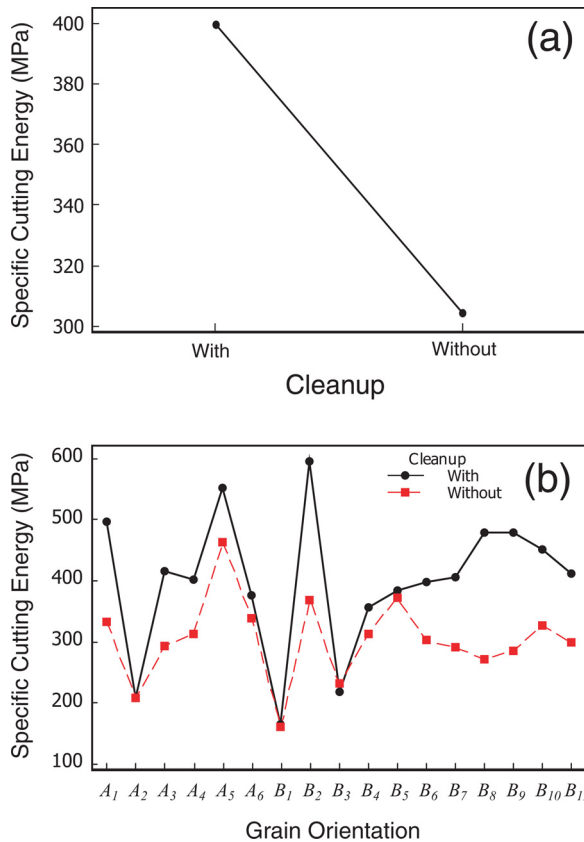


Fig. 15. (a) Main effect of cleanup cut and (b) two-way interaction effect for specific cutting energy between (a) the grain orientation and the cleanup cut.

rake angle and 250% at 25° rake angle. The interaction effect between the cutting velocity and orientation was seen to be statistically insignificant, indicating that the effect of velocity was uniform across all orientations for the range of velocities considered in this study. Furthermore, the well-known size effect was observed in all orientations, and the amount of size effect was seen to be orientation

dependent.

An equivalent coefficient of friction was calculated to facilitate analyzing different components of machining forces and different specific energies. The variation in the effective coefficient of friction (friction angle) was seen to be only between 4° to 5.7° for most crystallographic orientations. Based on the available data, when modeling the effects of anisotropy in machining, using a constant coefficient of friction could be a good approximation.

The crystallographic anisotropy was seen to strongly affect the surface roughness: The R_a values varies by as much as 831% due to crystallographic anisotropy. Furthermore, it is observed that the orientations that produce higher specific cutting energies result in higher surface roughnesses and increased uncut chip thicknesses exacerbated the effect of crystallographic anisotropy on surface roughness.

Comparing the results from the experiments without cleanup cuts to those with cleanup cuts, it was observed that the presence of larger subsurface deformation reduces the average (across cutting parameters and orientations) specific cutting energy. At lower rake angles, the effect of subsurface deformation was seen to be stronger: the specific cutting energies with cleanup cuts were higher by 8.7%, 29% and 45% at 25°, 10° and 0° rake angles, respectively. The effect of subsurface damage was also seen to be strongly depend upon the crystallographic orientation. The reduction in standard deviation of average specific cutting energy without the cleanup cuts (68 MPa), compared to the cleanup cuts (115 MPa), indicated that larger subsurface deformation reduces the effect of anisotropy. Lastly, the subsurface deformation was not seen to influence the effective coefficient of friction values significantly.

In summary, the specific cutting energy was seen to be correlated strongly with the rake angle, where a larger rake angle resulted in lower specific cutting energies (Fig. 9) and possibly in reduced sub-surface deformations. This follows the well-known results in macro-machining, and our results confirm that it equally applies to large-polycrystalline cutting. Overall, larger rake angles were also seen to reduce the effect of anisotropy on specific cutting energy (Fig. 10(a)). At lower rake angles, increased strains and larger shear zone, along with changes in the orientation of the shear deformation, could require activation of a large number of deformation planes within the crystals, resulting in increased variation in specific cutting energy with crystallographic orientation. Similarly, surfaces formed in such a complex deformation are likely to

induce degradation in surface finish at lower rake angles. As a result, larger rake angles are likely to produce a relatively stable cutting force across multiple grains, resulting in an improved surface finish (Fig. 13(e)).

Smaller uncut chip thicknesses were seen to reduce the effect of anisotropy (Fig. 13(f)). A larger uncut chip thickness results in an increased dislocation density on the machined surface, implying a higher plastic deformation [39]. A higher plastic deformation on the cutting plane could increase the effect of anisotropy on the surface, as evidenced by the increased surface roughness. Therefore, a few finishing cuts with lower uncut chip thickness is beneficial to reduce the effect of anisotropy and obtain superior surface finish. Lastly, the cleanup cuts had a significant effect on the specific cutting energy for most crystallographic orientations: this indicates the presence of sub-surface deformation. These sub-surface deformation changes the crystal orientation beneath the surface (e.g., via recrystallization) which could be equivalent to cutting a totally different grain(s) as compared to the previous cut. As a result, in the presence of extensive subsurface damage, the specific cutting energies are significantly different between two consecutive cuts over the same grains.

The future work will include a detailed study on the sub-surface deformation to provide more quantitative understanding of the extent and effect of the sub-surface deformation on polycrystalline micromachining.

Conflict of interest

The authors declare that there is no conflict of interest.

Acknowledgements

The authors would like to thank Prof. A. D. Rollett of Carnegie Mellon University, for valuable discussions and for providing the pure aluminum workpieces and J.E. Ledonne for his assistance in OIM of the workpiece. This work was supported by the National Science Foundation CAREER Program under award number CMMI-0547534 (Ozdoganlar).

References

- [1] Wu X, Li L, He N, Zhao M, Zhan Z. Investigation on the influence of material microstructure on cutting force and bur formation in the micro cutting of copper. *Int J Adv Manuf Technol* 2015;79(1–4):321–7. <https://doi.org/10.1007/s00170-015-6828-5>.
- [2] Ding X, Rahman M. A study of the performance of cutting polycrystalline Al 6061 T6 with single crystalline diamond micro-tools. *Precis Eng* 2012;36(4):593–603. <https://doi.org/10.1016/j.precisioneng.2012.04.009>.
- [3] Ding X, Jarfors AE, Lim GC, Shaw KC, Liu YC, Tang LJ. A study of the cutting performance of poly-crystalline oxygen free copper with single crystalline diamond micro-tools. *Precis Eng* 2012;36(1):141–52. <https://doi.org/10.1016/j.precisioneng.2011.09.001>.
- [4] Ramalingam S, Hazra J. Dynamic shear stress – analysis of single crystal machining studies. *J Eng Ind* 1973;95(4):939–44.
- [5] Cohen PH. The orthogonal in-situ machining of single and polycrystalline aluminum and copper [Ph.D. thesis]. 1982.
- [6] To S, Lee WB, Chan CY. Ultraprecision diamond turning of aluminium single crystals. *J Mater Process Technol* 1997;60:157–62. [https://doi.org/10.1016/S0924-0136\(96\)02617-9](https://doi.org/10.1016/S0924-0136(96)02617-9).
- [7] Williams JA, Horne JG. Crystallographic effects in metal cutting. *J Mater Sci* 1982;17:2618–24. <https://doi.org/10.1007/BF00543896>.
- [8] Koenig W, Spenrath N. The influence of the crystallographic structure of the substrate material on surface quality and cutting forces in micromachining. Springer; 1991.
- [9] Moriwaki T, Okuda K, Shen GJ. Study of ultraprecision orthogonal microdiamond cutting of single-crystal copper. *JSME Int J Ser C: Dyn Control Robot Des Manuf* 1993;36(3):400–6.
- [10] Sato M, Kato Y, Tsutiya K. Effects of crystal orientation on the flow mechanism in cutting aluminum single crystal. *Trans Jpn Inst Met* 1979;20(8):414–22.
- [11] Sato M, Yamazaki T, Shimizu Y, Takabayashi T. A study on the microcutting of aluminum single crystals. *JSME Int J Ser 3: Vib Control Eng Eng Ind* 1991;34(4):540–5.
- [12] Yuan ZJ, Yao YX, Zhou M. Effect of crystallographic orientation on cutting forces and surface quality in diamond cutting of single crystal. *CIRP Ann* 1994;43(1):39–42.
- [13] Lawson BL, Kota N, Ozdoganlar OB. Effects of crystallographic anisotropy on orthogonal micromachining of single-crystal aluminum. *J Manuf Sci Eng* 2008;130(3):0311161. <https://doi.org/10.1115/1.2917268>.
- [14] Sato M, Kato Y, Aoki S, Ikoma A. Effects of crystal orientation on the cutting mechanism of the aluminum single crystal: 2nd report: on the (111) plane and the (112) end cutting. *Bull JSME* 1983;26(215):890–6.
- [15] Clarebrough LM, Ogilvie GJ. Microstructure by machining, machining theory and practice. ASM; 1950. p. 110–21.
- [16] Von Turkovich BF, Black JT. Micro-machining of copper and aluminum crystals. *J Eng Ind* 1970;92(1):130–4. <https://doi.org/10.1115/1.3427697>.
- [17] Black JT. Plastic deformation in ultramicrotomy of copper and aluminum. 1969.
- [18] Zhang SJ, To S, Wang SJ, Zhu ZW. A review of surface roughness generation in ultra-precision machining. *Int J Mach Tools Manuf* 2015;91:76–95. <https://doi.org/10.1016/j.ijmachtools.2015.02.001>.
- [19] Kota N, Ozdoganlar OB. Orthogonal machining of single-crystal and coarse-grained aluminum. *J Manuf Process* 2012;14(2):126–34. <https://doi.org/10.1016/j.jmapro.2012.01.002>.
- [20] Nahata S, Picard YN, Kota N, Burak Ozdoganlar O. Experimental investigation of sub-surface deformation using EBSD in single crystal aluminum during orthogonal micromachining. *Microsc Microanal* 2014;20(S3):1472–3. <https://doi.org/10.1017/s143192761400909x>.
- [21] Bitans K, Brown RH. An investigation of the deformation in orthogonal cutting. *Int J Mach Tool Des Res* 1965;5(3):155–65.
- [22] Luca DA, Seo YW, Komanduri R. Effect of tool edge geometry on energy dissipation in ultraprecision machining. *CIRP Ann* 1993;42(1):83–6.
- [23] Drescher J. Scanning electron microscopic technique for imaging a diamond tool edge. *Precis Eng* 1993;15(2):112–4.
- [24] Evans C, Polvani R, Postle M, Rhorer R. Some observations on tool sharpness and sub-surface damage in single point diamond turning. In-process optical metrology for precision machining, vol. 802. 1987. p. 52–66.
- [25] Ikawa N, Donaldson RR, Komanduri R, König W, McKeown PA, Moriwaki T, et al. Ultraprecision metal cutting – the past, the present and the future. *CIRP Ann* 1991;40(2):587–94.
- [26] M'Saoubi R, Ryde L. Application of the EBSD technique for the characterisation of deformation zones in metal cutting. *Mater Sci Eng A* 2005;405(1–2):339–49. <https://doi.org/10.1016/j.msea.2005.06.002>.
- [27] Elmaliagli M, Alpas AT. Metallographic analysis of the deformation microstructure of copper subjected to orthogonal cutting. *Mater Sci Eng A* 2003;355(1–2):249–59. [https://doi.org/10.1016/S0921-5093\(03\)00072-8](https://doi.org/10.1016/S0921-5093(03)00072-8).
- [28] DeVor RE, Chang T-h, Sutherland JW. Statistical quality design and control: contemporary concepts and methods. Prentice Hall; 2007.
- [29] Sato M, Kato Y, Tsutiya K, Aoki S. Effects of crystal orientation on the cutting mechanism of aluminum single crystal. *Bull JSME* 1981;24(196):1864–70.
- [30] Sato M, Yamazaki T, Kubo M. The cutting mechanism of an aluminum single crystal based on the crystal slip theory. *Trans Jpn Inst Met* 1985;26(4):251–8.
- [31] Kota N, Ozdoganlar OB. A simplified model for orthogonal micromachining of fcc single-crystal materials. *Trans NAMRI/SME* 2008;36:193–200.
- [32] Kota N, Ozdoganlar OB. A model-based analysis of orthogonal cutting for single-crystal FCC metals including crystallographic anisotropy. *Mach Sci Technol* 2010;14(1):120–7. <https://doi.org/10.1080/10910340903586517>.
- [33] Shaw MC. The size effect in metal cutting. *Sadhana* 2003;28(5):875–96. <https://doi.org/10.1007/BF02703319>.
- [34] Melkote SN. An explanation for the size-effect in machining using strain gradient plasticity. *ASME J Manuf Sci Eng* 2004;126:679–84.
- [35] Dinesh D, Swaminathan S, Chandrasekar S, Farris TN. An intrinsic size-effect in machining due to the strain gradient. Proceedings of ASME IMECE, vol. 2001. 2001. p. 1–8.
- [36] Filiz S, Conley CM, Wasserman MB, Ozdoganlar OB. An experimental investigation of micro-machinability of copper 101 using tungsten carbide micro-endmills. *Int J Mach Tools Manuf* 2007;47(7–8):1088–100. <https://doi.org/10.1016/j.ijmachtools.2006.09.024>.
- [37] Atkins A. Modelling metal cutting using modern ductile fracture mechanics: quantitative explanations for some longstanding problems. *Int J Mech Sci* 2003;45(2):373–96. [https://doi.org/10.1016/s0020-7403\(03\)00040-7](https://doi.org/10.1016/s0020-7403(03)00040-7).
- [38] Subbiah S, Melkote SN. Evidence of ductile tearing ahead of the cutting tool and modeling the energy consumed in material separation in micro-cutting. *J Eng Mater Technol* 2007;129(2):321–31.
- [39] To S, Lee WB. Deformation behaviour of aluminium single crystals in ultraprecision diamond turning. *J Mater Process Technol* 2001;113(1–3):296–300. [https://doi.org/10.1016/S0924-0136\(01\)00667-7](https://doi.org/10.1016/S0924-0136(01)00667-7).